PROCEEDINGS A

royalsocietypublishing.org/journal/rspa

Research

Cite this article: Zurlo G, Destrade M. 2026 Straight-to-helicoid transition of twisted cords. *Proc. R. Soc. A* **482**: 20251044. https://doi.org/10.1098/rspa.2025.1044

Received: 2 December 2025
Accepted: 22 January 2026

Subject Areas:
mechanics, mathematical physics, applied mathematics

Keywords:
torsional instability, nonlinear elasticity, incompressibility, energy minimization, helical instability, rubber cords

Author for correspondence:
Giuseppe Zurlo
e-mail: giuseppe.zurlo@universityofgalway.ie

Straight-to-helicoid transition of twisted cords

Giuseppe Zurlo[1] and Michel Destrade[1,2]

[1]School of Mathematical and Statistical Sciences, University of Galway, University Road, Galway, Ireland
[2]Key Laboratory of Soft Machines and Smart Devices of Zhejiang Province, Department of Engineering Mechanics, Zhejiang University, Hangzhou 310027, People's Republic of China

GZ, 0000-0002-1438-5015; MD, 0000-0002-6266-1221

When a stretched rubber cord is twisted, it eventually develops elaborate instability patterns. For a sufficiently slender cord, the first step in this sequence is the emergence of helical shapes, which later destabilize into knots as the torque grows. Capturing this onset analytically is notoriously difficult owing to geometric and constitutive nonlinearities. Here, we present an energy-based route that focuses on the first transition: the formation of a helicoid from the straight, twisted state. By adopting reduced kinematics for a slender, volume-preserving, hyperelastic cord, we place straight and helicoidal configurations on the same footing under combined axial stretch and torsion. This reduction turns an otherwise differential problem into a purely algebraic one, allowing us to pinpoint the critical torsional load at which the transition occurs. A key advantage of this formulation is that it yields a fully analytical description of the post-buckled helicoidal state, valid even for arbitrarily large applied torque and axial pre-stretch. Beyond the instability threshold, the helicoidal amplitude grows smoothly with torque, while the pitch decreases; features consistent with our experiments and with previous observations.

1. Introduction

Elastic instabilities taking place in soft solids are often easy to produce with simple desktop experiments, and at the same time, are quite complex to model analytically. One such example concerns the twisting

THE ROYAL SOCIETY PUBLISHING

instabilities of an axially stretched rubber cord. This easy experiment reveals that, beyond a certain threshold of applied torque (below which the cord remains straight) the cord undergoes out-of-plane buckling. As the torque increases further, a remarkably rich variety of spatial configurations emerges, eventually including intricate and convoluted knotted patterns [1].

The ease of reproducing this instability may explain why it is so frequently exploited by Nature [2]. By invoking a few scale-spanning examples, we find that helicoidal instabilities are thought to be behind the biologically crucial processes of DNA knotting [3], protein folding [4], buckling under tension in actin filaments [5,6], active control of tendril perversions in climbing plants [7] and plant roots [8], and also part of technological processes where helical shapes are formed in the self-assembly of semiconductor nanoparticles [9].

The appealing beauty of the problem has attracted sustained interest in the mathematical community. Spurred on by Kirchhoff's initial programme to classify all possible helical equilibria of inextensible and unshearable rods [10], many have embraced his challenge. While, again, it is not easy to give an exhaustive account of this literature, a selection is possible by noting that a majority of works have confined the analysis to Cosserat rod theory or, in cases where the rod is assumed inextensible and unshearable, to Kirchhoff's elastic rod model, so that the complexity to deal with a three-dimensional body is effectively reduced by describing the rod through its centreline, upon which resultant forces and moments are applied, see [1,3,7,11–15].

In many practically relevant situations, particularly when dealing with soft solids capable of large deformations, the material behaviour is described by a three-dimensional constitutive law [16], from which it might be possible to address specific boundary value problems. Yet, this aim underscores the very limitation of the Cosserat or Kirchhoff models: their weak connection to the underlying three-dimensional constitutive behaviour of the material. These rod models are formulated directly in terms of strain measures associated with the rod's centreline, such as curvature and twist, and often assume a quadratic dependence on these quantities. While this assumption simplifies the analysis by reducing the complexity of the problem to geometric nonlinearities, it remains non-trivial to ensure that the resulting one-dimensional energy accurately reflects the full three-dimensional material response (see [17–21]). As remarked by Ericksen [22] about the existence of uniform states of elastic rods, '*it is impossible to say much … without introducing some assumptions concerning the form of the strain-energy density function*.'

Another degree of complexity arises because torsional instabilities in out-of-plane rods involve nonlinear differential equations, making the analysis highly technical or even impossible. The beauty of analytical solutions is, however, achievable if one renounces tackling the full picture and focuses instead on special features of the problem. Gent & Hua [23], for instance, studied the formation of a knot in a twisted, stretched hyperelastic cord by introducing strong but insightful simplifications to compare the energies of knotted and straight configurations, yielding a remarkably accurate prediction of the critical torque across various materials and geometries. A similar semi-inverse approach was used by Ericksen [22], who employed inverse assumptions to reduce complex differential problems to algebraic ones, allowing general conclusions on uniform states, such as helices in curved rods.

In this work, we do not attempt to capture the full complexity of the buckled states in twisted cords. From our experiments, see figure 1 and similar results in the literature, we have observed that as torque is gradually increased in a straight, axially pre-stretched cord, a critical torque is reached when helicoidal shapes start to emerge. The transition is *supercritical*, in the sense that the straight-to-helicoid transition takes place smoothly (as opposed to the *subcritical* transition towards the knotted configuration). When the cord is sufficiently slender, these helicoidal patterns feature nearly uniform wavelength and amplitude, except for a narrow region close to the clamped ends. With further increase of the torque, the helicoid becomes more tightly wound, and its wavelength decreases while the amplitude grows, until more intricate forms of instability emerge [24].

Focusing on incompressible and hyperelastic materials, we investigate the onset of the straight-to-helicoid transition by introducing a family of uniform helicoidal configurations and computing their total potential energy. This approach reduces the stability analysis to a purely algebraic

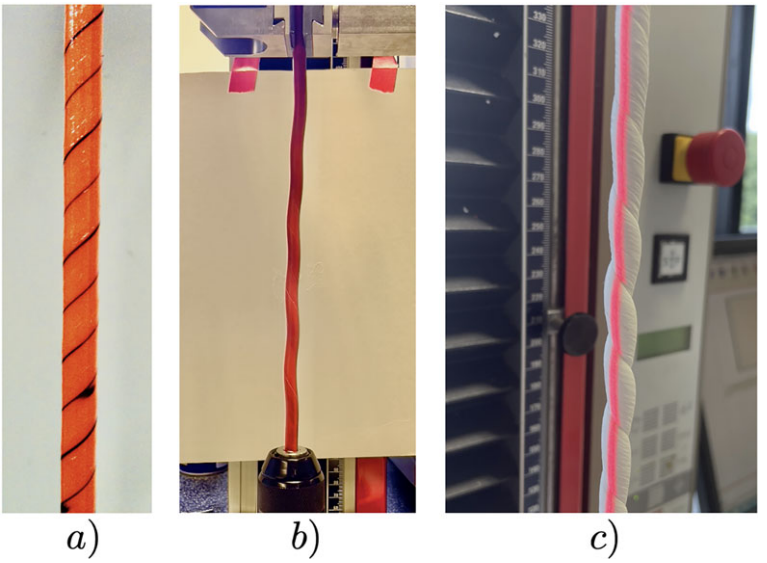

Figure 1. (*a*,*b*) Twisting of an incompressible silicone cord: at first, the cord remains straight as the pitch increases; then it transitions into a helicoid. (*c*) Twisting of a compressible foam cord: self contacts develop in the twisted cord, highlighted by a laser beam aligned with the axis.

problem, where the unknowns are the axial stretch λ of the centreline, the centreline curvature κ, the centreline torsion τ and the excess twist γ. Notably, this family of helicoids includes the straight, twisted cord as a special case. We minimize the total potential energy within this class of deformations, subject to the constraint that the current height of the cord is prescribed, a condition that induces a non-trivial constraint manifold among the variables involved [15].

Our analysis reveals that, for a broad range of material responses, the straight twisted configuration remains energetically favourable compared to helicoids, up to a critical torque. Beyond this threshold, helicoidal shapes become energetically preferable. Remarkably, this same critical torque also marks the point at which the straight configuration loses stability with respect to helicoidal perturbations. As the torque increases beyond this initial threshold, the helicoid's amplitude grows while its pitch decreases smoothly, in agreement with experimental observations. Note that the stability analysis presented in this work is performed within the class of uniform helicoidal perturbations, so that the resulting loss of stability of the straight configuration should be interpreted as conditional within this restricted ansatz.

As with Gent & Hua's estimate for the formation of the first knot in a twisted cord [23], our prediction for the straight-to-helicoid transition reduces to a simple analytical expression. Taken together, their estimate and ours define the upper and lower bounds of a region in the space of control parameters where a rich variety of non-straight, non-knotted configurations can arise. Within this intermediate regime, algebraic approaches like those employed here and in [23] are unlikely to yield further insights, as the system is expected to exhibit non-homogeneous configurations, strongly dominated by boundary effects [24], scenarios that require the use of highly nonlinear differential equations and rather advanced techniques [25,26].

Focusing on incompressible and hyperelastic materials, we are also able to establish a connection with another key feature of twisted cords: the Poynting effect, i.e. the tendency of cylinders to lengthen axially when twisted [27]. This connection is particularly relevant to our setting, where the cord is axially pre-stretched and subsequently constrained in height before twisting. One might suspect that the straight-to-helicoid transition is triggered by the onset of axial compressive forces owing to the Poynting effect. However, we show that for a broad class of material behaviours, the instability occurs while the cord remains under tension. It is important to

note that such an estimate would not be accessible through director theories, which are inherently unable to capture the Poynting effect.

In short, the paper develops an energy-based framework to capture the straight-to-helicoid transition in twisted, axially pre-stretched cords, with explicit connections to the Poynting effect and comparisons to experimental data. It is organized as follows. In §2, we derive the energy of an approximately incompressible helicoid and introduce our ansatz. In §3, we present the constrained minimization procedure and the stability analysis, for the neo-Hookean case and with extension to Mooney–Rivlin materials. In §4, we compare the theoretical predictions with experimental data from the literature. Finally, in §5, we conclude with a discussion of the main findings, their limitations, and perspectives for future research.

2. Energy of an approximately incompressible helicoid

Here we derive the energy of an approximately incompressible, stretched and twisted helical cord. We then develop an energetic framework accounting for the Poynting effect (the tendency of cords to lengthen in torsion) and for the transition from straight to helicoidal shape, a phenomenon commonly observed in torsion experiments of cords, prior to the formation of knots.

We call $\mathcal{R}_0$ the reference, unstressed configuration of the cord as a right cylinder with circular cross-section, with points parameterized in cylindrical coordinates R, θ, Z through

$$\boldsymbol{X}(R,\theta,Z) = R\boldsymbol{E}_R(\theta) + Z\boldsymbol{k}, \quad R \in (0,A),\ Z \in (0,H),\ \theta \in (0,2\pi), \tag{2.1}$$

where A and H are, respectively, the radius and height of the reference configuration of the cord, where the referential radial and hoop unit vectors are defined as

$$\boldsymbol{E}_R = \cos\theta\boldsymbol{i}_1 + \sin\theta\boldsymbol{i}_2 \quad \text{and} \quad \boldsymbol{E}_\theta = -\sin\theta\boldsymbol{i}_1 + \cos\theta\boldsymbol{i}_2, \tag{2.2}$$

and $\{\boldsymbol{i}_1, \boldsymbol{i}_2, \boldsymbol{i}_3\}$ is a fixed orthonormal basis, with $\boldsymbol{i}_3 \equiv \boldsymbol{k}$ coinciding with the axis of the cord, see figure 2.

In its current configuration $\mathcal{R}$, the cord is an axially stretched, regular helicoid, with its centreline represented by the helical curve

$$\boldsymbol{c}(Z) = Q\boldsymbol{e}_r(Z) + P\delta Z\boldsymbol{k}, \tag{2.3}$$

where Q is the radial distance of the centreline from the axis of the helix, and where we now introduce the radial and hoop unit vectors,

$$\boldsymbol{e}_r(Z) = \cos(\delta Z)\boldsymbol{i}_1 + \sin(\delta Z)\boldsymbol{i}_2 \quad \text{and} \quad \boldsymbol{v}(Z) = -\sin(\delta Z)\boldsymbol{i}_1 + \cos(\delta Z)\boldsymbol{i}_2, \tag{2.4}$$

respectively. The parameters (δ, Q, P) introduced above can be computed from the stretch, curvature and torsion of the deformed centreline. To this end, we introduce the local triad of tangent $\boldsymbol{t}$, normal $\boldsymbol{n}$ and binormal $\boldsymbol{b}$ unit vectors to the helicoidal centreline,

$$\boldsymbol{t} = \frac{\boldsymbol{c}'}{||\boldsymbol{c}'||} = \frac{Q\boldsymbol{v} + P\boldsymbol{k}}{\sqrt{P^2+Q^2}}, \quad \boldsymbol{n} = \frac{\boldsymbol{c}''}{||\boldsymbol{c}''||} = -\boldsymbol{e}_r \quad \text{and} \quad \boldsymbol{b} = \boldsymbol{t}\times\boldsymbol{n} = \frac{-P\boldsymbol{v} + Q\boldsymbol{k}}{\sqrt{P^2+Q^2}}, \tag{2.5}$$

so that the stretch λ, curvature κ, and torsion τ of the centreline curve are

$$\left.\begin{aligned} &\lambda = ||\boldsymbol{c}'|| = \delta\sqrt{P^2+Q^2}, \quad \kappa = \boldsymbol{t}'\cdot\boldsymbol{n} = \frac{Q\delta}{\sqrt{P^2+Q^2}} \\ \text{and} \quad &\tau = -\boldsymbol{b}'\cdot\boldsymbol{n} = \frac{P\delta}{\sqrt{P^2+Q^2}}, \end{aligned}\right\} \tag{2.6}$$

respectively. By inverting these expressions, we obtain

$$\delta = \sqrt{\kappa^2+\tau^2}, \quad P = \frac{\lambda\tau}{\kappa^2+\tau^2} \quad \text{and} \quad Q = \frac{\lambda\kappa}{\kappa^2+\tau^2}, \tag{2.7}$$

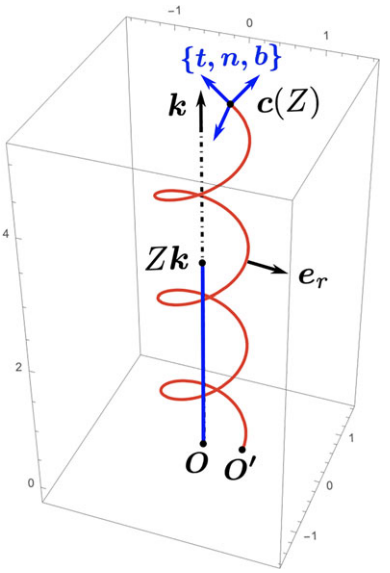

Figure 2. With **k** unit vector along the axis of the straight reference configuration of the undeformed helicoid (blue), a point $Z\mathbf{k}$ in the reference centreline is mapped into a point $\mathbf{c}(Z)$ in the current centreline of the deformed helicoid (red). Also represented here are the radial unit vector $\mathbf{e}_r$ in the reference configuration, and the triad (**t, n, b**) of tangent, normal and binormal in the current configuration.

and it follows that the equation of the deformed centreline is

$$\boldsymbol{c}(Z) = \frac{\lambda\kappa}{\kappa^2+\tau^2}\boldsymbol{e}_r(Z) + \frac{\lambda\tau}{\sqrt{\kappa^2+\tau^2}}Z\boldsymbol{k}, \tag{2.8}$$

see figure 2 for an illustration of the main features of the resulting helicoid. For definiteness, we consider right-handed helices: $\tau \geq 0$, and we also assume that $\kappa \geq 0$. The current height of the deformed centreline is (see figure 2)

$$h = z(H) = \boldsymbol{c}(H)\cdot\boldsymbol{i}_3 = \frac{\lambda\tau H}{\sqrt{\kappa^2+\tau^2}}. \tag{2.9}$$

From this expression, we see that when the grips at the end of the cord are kept at a constant distance from each other during torsion, $h = H$ and

$$\lambda = \frac{\sqrt{\kappa^2+\tau^2}}{\tau} \geq 1, \tag{2.10}$$

so that, as expected, the deformed centreline is stretched. Calling α the angle between the centreline tangent $\boldsymbol{t}$ and the helix axis $\boldsymbol{k}$, we have

$$\tan\alpha = \frac{\kappa}{\tau}, \tag{2.11}$$

showing the limits of the helix degenerating into a closed ring ($\alpha \to \pi/2$) for vanishing torsion ($\tau \to 0$) with curvature ($\kappa > 0$) and into a straight twisted cord ($\alpha \to 0$) for vanishing curvature ($\kappa \to 0$) with torsion ($\tau > 0$).

Finally, we record that the centreline *pitch* of the helix is $L = 2\pi/\delta$ (measured in the reference configuration) and the *semi-amplitude* is $R = \lambda\kappa/(\kappa^2+\tau^2)$.

We now construct an *ansatz* describing three-dimensional helicoids with centreline given by equation (2.8). Specifically, we assume that cross-sections $Z =$ constant in $\mathcal{R}_0$ remain circular, flat and perpendicular to the deformed centreline in the current configuration $\mathcal{R}$, but may undergo a rigid rotation in the local tangent plane spanned by $\{\boldsymbol{n}, \boldsymbol{b}\}$. To describe this rotation we introduce

royalsocietypublishing.org/journal/rspa Proc. R. Soc. A 482: 20251044

the *excess twist* γ, assumed uniform (see [12,13]), and the *register angle* $\varphi = \theta + \gamma Z$, so that a fibre in direction $\boldsymbol{E}_R(\theta)$ in $\mathcal{R}_0$ is mapped to the fibre (also called *director*):

$$\boldsymbol{d}(\theta, Z) = \cos(\theta + \gamma Z)\boldsymbol{n}(Z) + \sin(\theta + \gamma Z)\boldsymbol{b}(Z), \tag{2.12}$$

in $\mathcal{R}$. Our *ansatz* for the formation of the helicoid is

$$\boldsymbol{\chi}(R, \theta, Z) = \boldsymbol{c}(Z) + \lambda_R R\, \boldsymbol{d}(\theta, Z), \tag{2.13}$$

mapping points $\boldsymbol{X} = R\boldsymbol{E}_R(\theta) + Z\boldsymbol{k}$ in $\mathcal{R}_0$ into points $\boldsymbol{x} = \boldsymbol{\chi}(\boldsymbol{X})$ in $\mathcal{R}$, where λ_R is the stretch in the radial direction, and is assumed constant.

We wish to model cords made of rubber, which, by and large, is incompressible. As we now show, it is not possible to enforce incompressibility pointwise with equation (2.13); it would require a broader class of deformations, capable of describing warped, possibly non-circular cross-sections, while yielding a significant burden for the analytical treatment, see [28,29]. Instead, we content ourselves with enforcing incompressibility *on average* for each cross-section of the cylinder (see [17, §16.12] for a detailed discussion on incompressibility in the context of rod theories). First, we impose

$$\lambda_R = \lambda^{-1/2}, \tag{2.14}$$

a relation that would be expected were the incompressible right cylinder to remain straight during deformation. Then, using equations (2.12) and (2.13), we compute the right Cauchy–Green tensor $\mathbf{C} = \mathbf{F}^{\mathrm{T}}\mathbf{F}$ of the deformation gradient $\mathbf{F} = \nabla\boldsymbol{\chi}$, as

$$\mathbf{C} = \lambda^{-1}(\boldsymbol{E}_R \otimes \boldsymbol{E}_R + \boldsymbol{E}_\theta \otimes \boldsymbol{E}_\theta) + \left(\frac{R}{H}\right)(\gamma + \tau)(\boldsymbol{E}_\theta \otimes \boldsymbol{k} + \boldsymbol{k} \otimes \boldsymbol{E}_\theta) + \lambda_Z \boldsymbol{k} \otimes \boldsymbol{k}, \tag{2.15}$$

where $\lambda_Z = \lambda_Z(R, \theta, Z)$, and the inhomogeneous stretch in the Z direction (not to be confused with λ, the stretch along the deformed axis of the cord) is

$$\lambda_Z = \frac{1}{2\lambda}\{\lambda^3 + R^2[\kappa^2 + 2(\gamma + \tau)^2] - R\kappa[4\lambda^{3/2}\cos(\gamma Z + \theta) - R\kappa\cos 2(\gamma Z + \theta)]\}. \tag{2.16}$$

From these expressions we compute

$$\det \mathbf{C} = [1 - \lambda^{-3/2} R\kappa \cos(\gamma Z + \theta)]^2, \tag{2.17}$$

making it clear that $\det \mathbf{C} \neq 1$ in general. However, the average of $\det \mathbf{C}$ over a referential cross-section $Z =$constant is

$$\langle \det \mathbf{C} \rangle_{Z=\text{const}} = \frac{1}{\pi A^2} \int_0^{2\pi} \int_0^A (\det \mathbf{C}) R \, \mathrm{d}R \, \mathrm{d}\theta = 1, \tag{2.18}$$

confirming that incompressibility is satisfied on average by the ansatz equation (2.13), see for example [30,31] for similar assumptions.

Note that the factor $\lambda^{-3/2} R\kappa$ in equation (2.17), which gives rise to local deviations from exact incompressibility, is typically small when $R\kappa \ll \lambda^{3/2}$. Consequently, higher axial pre-stretch reduces these deviations, even for thicker or more curved cords, therefore the approximated theory presented here is expected to provide more accurate estimates for cords with higher axial pre-stretch.

We are now in a position to derive the energy of the helicoid as a function of the parameters (λ, κ, τ). We take the Mooney–Rivlin energy for the material model because it covers, at the same level of approximation, the most general form of third-order incompressible elasticity. Hence the volumetric strain energy density is

$$W = C_1(I_1 - 3) + C_2(I_2 - 3), \tag{2.19}$$

where $I_1 = \operatorname{tr} \mathbf{C}$ and $I_2 = \frac{1}{2}[(\operatorname{tr} \mathbf{C})^2 - \operatorname{tr} \mathbf{C}^2]$ are the two first two principal invariants of $\mathbf{C}$, and C_1, C_2 are positive constitutive parameters. The connection with weakly nonlinear incompressible isotropic elasticity is that $2(C_1 + C_2) = \mu$, the shear modulus of linear elasticity, and $-8(C_1 + 2C_2) = \mathcal{A}$, the third-order Landau constant [32].

royalsocietypublishing.org/journal/rspa Proc. R. Soc. A 482: 20251044

Upon integration over the reference configuration we obtain the total energy in the cord as

$$E = \int_0^H \int_0^{2\pi} \int_0^A WR\,\mathrm{d}R\,\mathrm{d}\theta\,\mathrm{d}Z = \pi H A^2 w, \tag{2.20}$$

where w is of the form

$$w = w_0 + w_1 A^2, \tag{2.21}$$

with

$$\left.\begin{aligned} w_0 &= C_1(\lambda^2 + 2\lambda^{-1} - 3) + C_2(\lambda^{-2} + 2\lambda - 3) \\ \text{and}\quad w_1 &= \frac{1}{4\lambda^2}\{C_1\lambda[\kappa^2 + 2(\tau+\gamma)^2] + 2C_2[\kappa^2 + (\gamma+\tau)^2]\}. \end{aligned}\right\} \tag{2.22}$$

Here, the leading-order term w_0 is the energy of an axially stretched straight cylinder, while the higher-order term $A^2 w_1$ represents the energy owing to the combined actions of twist, curvature and stretch.

A fundamental feature of the energy equation (2.21) is that it cannot be trivially obtained from general phenomenological expressions of the constitutive laws for elastic rods based on Cosserat theory (see §5.3 in [12]). Specifically, we note the non-trivial dependency of the energy on the curvature κ and the *twist density* $u_3 = \tau + \gamma$.

In what follows, we first treat the special case of neo-Hookean solids, where $C_2 = 0$, explicitly. The derivation for Mooney–Rivlin solids ($C_2 > 0$) is presented in §3c.

3. Constrained energy minimization and stability

For the neo-Hookean model, we have $C_1 = \mu/2$, $C_2 = 0$, and the energy per unit reference length is

$$\frac{E}{H} = \mu\left[\frac{\Omega}{2}(\lambda^2 + 2\lambda^{-1} - 3) + \frac{J_b}{2}\left(\frac{\kappa}{\sqrt{\lambda}}\right)^2 + \frac{J_o}{2}\left(\frac{u_3}{\sqrt{\lambda}}\right)^2\right], \tag{3.1}$$

where we set $\Omega = \pi A^2$, $J_b = \pi A^4/4$ and $J_o = \pi A^4/2$ for the cross-sectional area, the flexural moment of inertia and the torsional moment of inertia in the undeformed configuration, respectively.

As the bending moment M_b, torque M_t and axial traction F are the work conjugates of curvature κ, twist density $u_3 = \tau + \gamma$ and axial stretch λ, respectively, we find that for the neo-Hookean cord equation (3.1),

$$\left.\begin{aligned} M_t &= \frac{\partial E/H}{\partial u_3} = \mu J_o \frac{u_3}{\lambda}, \\ M_b &= \frac{\partial E/H}{\partial \kappa} = \mu J_b \frac{\kappa}{\lambda} \\ \text{and}\quad F &= \frac{\partial E/H}{\partial \lambda} = \mu\Omega\left(\lambda - \frac{1}{\lambda^2} - \frac{A^2}{4}\frac{u_3^2}{\lambda^2} - \frac{A^2}{8}\frac{\kappa^2}{\lambda^2}\right). \end{aligned}\right\} \tag{3.2}$$

Introducing the following non-dimensional deformation quantities:

$$\tilde{\kappa} = \kappa A, \quad \tilde{\tau} = \tau A, \quad \tilde{\gamma} = \gamma A \quad \text{and} \quad \tilde{u}_3 = u_3 A = (\tilde{\gamma} + \tilde{\tau}), \tag{3.3}$$

non-dimensional static quantities,

$$m_b = \frac{M_b}{(\mu\pi A^3)}, \quad m_t = \frac{M_t}{(\mu\pi A^3)} \quad \text{and} \quad f = \frac{F}{\mu\pi A^2} \tag{3.4}$$

and non-dimensional energy,

$$e = \frac{E}{\mu H \pi A^2} = \frac{1}{2}(\lambda^2 + 2\lambda^{-1} - 3) + \frac{1}{8}\lambda^{-1}\tilde{\kappa}^2 + \frac{1}{4}\lambda^{-1}\tilde{u}_3^2, \tag{3.5}$$

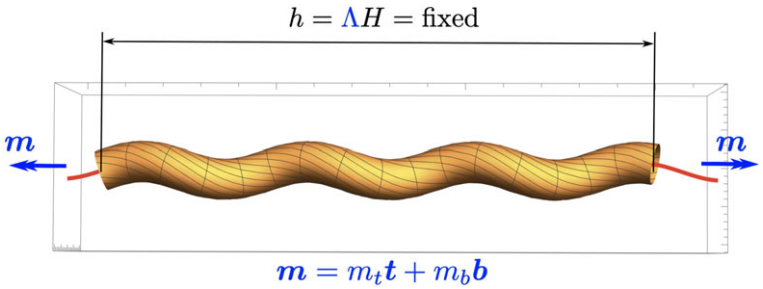

Figure 3. A specimen of the twisted cord in its current configuration, under the action of torque couples $\pm m\mathbf{k}$, acting along the undeformed centreline. As the straight cord transitions to helicoid, the applied torques give rise to bending (m_b) and torsion (m_t) components relative to the deformed centreline. Because the deformed helicoid is uniform, it is assumed that during the application of the torque, the ratio $\Lambda = h/H$ between the current height and reference height of the cord is fixed.

we obtain

$$\left.\begin{aligned} m_b &= \frac{\partial e}{\partial \tilde{\kappa}} = \frac{1}{4}\lambda^{-1}\tilde{\kappa}, \quad m_t = \frac{\partial e}{\partial \tilde{u}_3} = \frac{1}{2}\lambda^{-1}(\tilde{\tau}+\tilde{\gamma}) \\ \text{and} \qquad f &= \frac{\partial e}{\partial \lambda} = \lambda - \lambda^{-2} - \frac{1}{8}\lambda^{-2}\tilde{\kappa}^2 - \frac{1}{4}\lambda^{-2}(\tilde{\tau}+\tilde{\gamma})^2. \end{aligned}\right\} \tag{3.6}$$

We now proceed with minimizing the elastic energy under suitable controls. Specifically, we model experiments where the cord is pre-stretched axially, before an increasing torque is applied. Here, a word of caution is in order relative to the boundary conditions: by minimizing the elastic energy equation (3.5) within the class of deformations equation (2.13), we cannot impose that the end faces of the cord are perpendicular to $\boldsymbol{k}$: in fact, this condition is incompatible with the ansatz equation (2.13), and would imply that inhomogeneous deformations arise at the onset of instability. Addressing such effects in slender cords necessitates an asymptotic theory that incorporates inhomogeneous deformations, leading to the study of highly nonlinear ordinary differential equations. These considerations exceed the scope of our approximations and are left for future work.

Here, we look for minimizers of the elastic energy equation (3.5) when (i) the ratio $\Lambda = h/H$ is prescribed and (ii) the uniform axial torque $\boldsymbol{m} = m\,\boldsymbol{k}$ is prescribed, see figure 3. Because the torque $\boldsymbol{m}$ lies in the $(\boldsymbol{b},\boldsymbol{t})$-plane (recall that $\boldsymbol{n} = -\boldsymbol{e}_r$ is perpendicular to $\boldsymbol{k}$ [1]), the axial torque may be decomposed into the components:

$$m_b = \boldsymbol{m}\cdot\boldsymbol{b} = m\,\boldsymbol{k}\cdot\boldsymbol{b} \quad \text{and} \quad m_t = \boldsymbol{m}\cdot\boldsymbol{t} = m\,\boldsymbol{k}\cdot\boldsymbol{t}. \tag{3.7}$$

We then introduce the non-dimensional *total potential energy*,

$$\mathcal{F}'(\lambda,\tilde{\kappa},\tilde{u}_3) = e(\lambda,\tilde{\kappa},\tilde{u}_3) - m_b\tilde{\kappa} - m_t\tilde{u}_3, \tag{3.8}$$

and we consider the minimization problem:

$$\min_{\lambda,\tilde{\kappa},\tilde{\tau},\tilde{\gamma}} \mathcal{F}', \quad \text{for } (\lambda,\tilde{\kappa},\tilde{\tau},\tilde{\gamma}) \text{ such that } \frac{\lambda\tilde{\tau}}{\sqrt{\tilde{\kappa}^2+\tilde{\tau}^2}} = \Lambda. \tag{3.9}$$

Note that the prescription of the ratio $\Lambda = h/H$ places a constraint only on $(\lambda,\tilde{\kappa},\tilde{\tau})$, which are deformation features of the centreline, while the elastic energy depends on $(\lambda,\tilde{\kappa},\tilde{\tau}+\tilde{\gamma})$, because the excess twist $\tilde{\gamma}$ is a feature of the three-dimensional helicoid only.

The constraint on the axial elongation of the cord can, however, be inverted to determine λ as a function of $\tilde{\kappa}$ and $\tilde{\tau}$, so that we may look for minimizers of the (now unconstrained) functional

$$\mathcal{F}(\tilde{\kappa},\tilde{\tau},\tilde{\gamma}) = \mathcal{F}'\left(\frac{\Lambda\sqrt{\tilde{\kappa}^2+\tilde{\tau}^2}}{\tilde{\tau}},\tilde{\kappa},\tilde{\tau}+\tilde{\gamma}\right), \tag{3.10}$$

where $\tilde{\kappa},\tilde{\tau},\tilde{\gamma}$ are considered as free variables.

(a) Straight cords and the Poynting effect

Recall that, as shown by Rivlin [33] and consistently with equations (3.2), the following normal force is required to keep a neo-Hookean cylinder under the stretch Λ and twist γ (per unit length of the unstretched rod):

$$F = \mu\pi A^2\left(\Lambda - \Lambda^{-2} - \frac{1}{4}\gamma^2\Lambda^{-2}A^2\right). \tag{3.11}$$

According to this formula, the force can in principle go from tensile ($F > 0$) to compressive ($F < 0$) for a fixed stretch and a large enough torsion. However, as we see in the next section, this does not happen because the cord transitions first to a helicoid, so that the torsion deformation underlying equation (3.11) is no longer valid.

The methodology devised in the paper can be specialized to the behaviour of a straight cord with axial pre-stretch Λ, subjected to the torque m. Because here, $\tilde{\kappa} = 0$, $\tilde{\tau} = 0$, it follows that $m_b = 0$, $m_t \equiv m$, $\tilde{u}_3 = \tilde{\gamma}$.

To determine the axial traction in the cord, we introduce a Lagrange multiplier f to enforce the constraint that the axial stretch λ equals the prescribed value $\Lambda > 1$. Therefore f may be interpreted as tension in the cord. The total potential energy equation (3.10) reads

$$\mathcal{F}(\lambda, \tilde{\gamma}) = \frac{1}{2}(\lambda^2 + 2\lambda^{-1} - 3) + \frac{1}{4}\lambda^{-1}\tilde{\gamma}^2 - f(\lambda - \Lambda) - m\tilde{\gamma}. \tag{3.12}$$

The stationarity conditions,

$$\frac{\partial\mathcal{F}}{\partial\lambda} = 0, \quad \frac{\partial\mathcal{F}}{\partial f} = 0 \quad \text{and} \quad \frac{\partial\mathcal{F}}{\partial\tilde{\gamma}} = 0, \tag{3.13}$$

give

$$\lambda - \lambda^{-2} = f + \frac{1}{4}\lambda^{-2}\tilde{\gamma}^2, \quad \lambda = \Lambda \quad \text{and} \quad m = \frac{1}{2}\lambda^{-1}\tilde{\gamma}, \tag{3.14}$$

respectively, and by eliminating λ and $\tilde{\gamma}$, we arrive at

$$\Lambda - \Lambda^{-2} = f + m^2. \tag{3.15}$$

This equation dictates that the axial load remains tensile ($f > 0$) as long as

$$m < m_P := \sqrt{\Lambda - \Lambda^{-2}}, \tag{3.16}$$

in agreement with equation (3.11). In the next section, we show that at the onset of the helicoidal instability, the critical torque m_{cr} is lower than m_P, meaning that straight-to-helicoid instability occurs while the cord is under tension.

Note that the minimum total potential energy is

$$\mathcal{F}_{\mathrm{straight}} = \frac{1}{2}(\Lambda^2 + 2\Lambda^{-1} - 3) - m^2\Lambda. \tag{3.17}$$

(b) Straight-to-helicoid transition: neo-Hookean materials

We first explore the equilibrium and the stability of the straight and helicoidal configurations for the neo-Hookean material, because calculations are transparent and compact for this model. We extend the methodology to other material models in §3c.

It is convenient to recast the analysis in terms of the parameter α introduced in equation (2.11), denoting the angle between the centreline tangent $\boldsymbol{t}$ and the helicoid axis $\boldsymbol{k}$. It is related to centreline curvature and torsion through $\kappa/\tau = \tan\alpha$, and to the applied torque m about $\boldsymbol{k}$ through $m_b = m\sin\alpha$, $m_t = m\cos\alpha$. The energy equation (3.10), now written as a function of $\tilde{\gamma}$, $\tilde{\tau}$ and α,

reads

$$\bar{\mathcal{F}}(\tilde{\gamma},\tilde{\tau},\alpha)=\frac{1}{8}\Lambda^{-1}[(8-8m\Lambda\tilde{\gamma}+2\tilde{\gamma}^2+4\tilde{\tau}\tilde{\gamma}+\tilde{\tau}^2)\cos\alpha \\ +(\tilde{\tau}^2-8m\Lambda\tilde{\tau})\sec\alpha+4\Lambda^3\sec^2\alpha-12\Lambda], \tag{3.18}$$

and stationary solutions correspond to

$$\frac{\partial\bar{\mathcal{F}}}{\partial\tilde{\gamma}}=\frac{\partial\bar{\mathcal{F}}}{\partial\tilde{\tau}}=\frac{\partial\bar{\mathcal{F}}}{\partial\alpha}=0. \tag{3.19}$$

Note that the first of these equations gives

$$\tilde{\gamma}=\tilde{\gamma}_h:=2m\Lambda-\tilde{\tau}, \tag{3.20}$$

and that for $0<\alpha<\pi/2$ (discarding $\alpha=0$ for a straight cord and $\alpha=\pi/2$ for a ring),

$$\frac{\partial^2\bar{\mathcal{F}}}{\partial\tilde{\gamma}^2}=\frac{1}{2}\Lambda^{-1}\cos\alpha>0. \tag{3.21}$$

Now we can look for minimizers of the function $\tilde{\mathcal{F}}(\tilde{\tau},\alpha)=\bar{\mathcal{F}}(\tilde{\gamma}_h,\tilde{\tau},\alpha)$, which read,

$$\tilde{\mathcal{F}}(\tilde{\tau},\alpha)=(\Lambda^{-1}-m^2\Lambda)\cos\alpha+\frac{1}{2}\Lambda^2\sec^2\alpha+\frac{\tilde{\tau}(\tilde{\tau}-8m\Lambda)}{8\Lambda}\frac{\sin^2\alpha}{\cos\alpha}-\frac{3}{2}. \tag{3.22}$$

Stationarity gives

$$\left.\begin{aligned}\frac{\partial\tilde{\mathcal{F}}}{\partial\tilde{\tau}}&=\left(\frac{1}{4}\Lambda^{-1}\tilde{\tau}-m\right)\frac{\sin^2\alpha}{\cos\alpha}=0\\ \text{and}\qquad\frac{\partial\tilde{\mathcal{F}}}{\partial\alpha}&=\frac{1}{8}\Lambda^{-1}\frac{\sin\alpha}{\cos^3\alpha}[(\tilde{\tau}^2-8m\Lambda\tilde{\tau}+8m^2\Lambda^2-8)\cos^3\alpha\\ &\quad+\tilde{\tau}(\tilde{\tau}-8m\Lambda)\cos\alpha+8\Lambda^3]=0.\end{aligned}\right\} \tag{3.23}$$

These equations define the *helicoid* as: $\alpha=\alpha_h$, $\tilde{\tau}=\tilde{\tau}_h$, with

$$\tilde{\tau}_h=4m\Lambda\quad\text{and}\quad\alpha_h=\arccos\left[\frac{D(m,\Lambda)}{6^{1/3}(1+m^2\Lambda^2)}-\frac{m^2\Lambda^2}{(3/2)^{1/3}D(m,\Lambda)}\right], \tag{3.24}$$

where we introduced the function

$$D(m,\Lambda)=\Lambda\left[9(1+m^2\Lambda^2)^2+\sqrt{3(1+m^2\Lambda^2)^3(27+32m^6+27m^2\Lambda^2)}\right]^{1/3}. \tag{3.25}$$

Note that α_h is defined uniquely because the cubic in the second of equations (3.23) has only one real root.

The analytical expression of the angle α_h which, we recall, defines the slope of the tangent to the helicoid's centreline relative to its axis, holds for arbitrarily large values of the applied torque m and axial pre-stretch Λ. As shown in figure 4, $\alpha_h=0$ when the applied torque reaches the critical value,

$$m_{\mathrm{cr}}(\Lambda)=\frac{\sqrt{\Lambda-\Lambda^{-2}}}{\sqrt{3}}. \tag{3.26}$$

As detailed below, when $m<m_{\mathrm{cr}}(\Lambda)$ the straight cord is stable and $\alpha_h=0$, whereas when $m>m_{\mathrm{cr}}(\Lambda)$ the angle α_h increases smoothly with the torque, underpinning a *supercritical* pitchfork-like bifurcation from the straight to the helicoidal state.

We now determine the range of controls (m,Λ) for which the stationary states found above are also energy minimizers, using the Hessian matrix of the energy equation (3.22),

$$\mathcal{H}(\tilde{\tau},\alpha)=\begin{bmatrix}\tilde{\mathcal{F}}_{,\tilde{\tau}\tilde{\tau}}(\tilde{\tau},\alpha) & \tilde{\mathcal{F}}_{,\tilde{\tau}\alpha}(\tilde{\tau},\alpha)\\ \tilde{\mathcal{F}}_{,\alpha\tilde{\tau}}(\tilde{\tau},\alpha) & \tilde{\mathcal{F}}_{,\alpha\alpha}(\tilde{\tau},\alpha)\end{bmatrix}, \tag{3.27}$$

where the comma denotes partial derivatives.

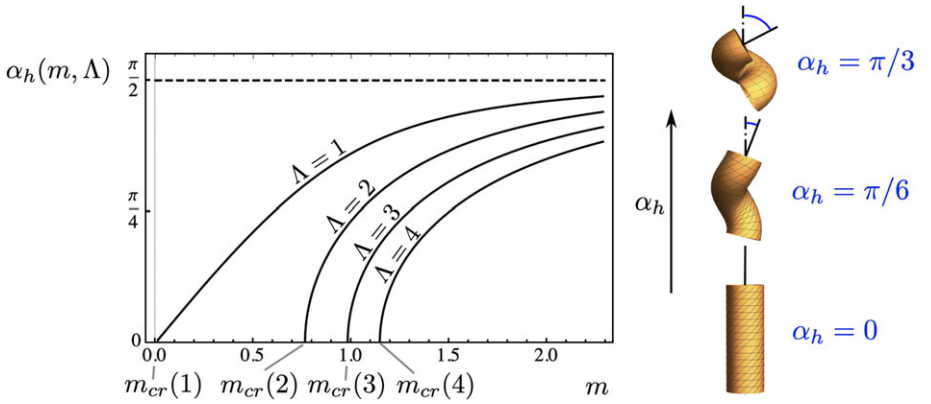

Figure 4. Slope of the helicoid's centreline α_h as a function of the applied torque m and of the axial pre-stretch Λ for neo-Hookean cords. Specifically, for $\Lambda > 1$, the centreline is straight ($\alpha_h = 0$) for all values of the torque below the critical torque $m_{\rm cr}(\Lambda)$, whereas the cord smoothly buckles toward helicoidal states past the critical torque (supercritical transition).

(i) Loss of stability of the straight configuration

When analysed within the class of helicoidal configurations, the straight configuration corresponds to $\alpha = 0$. Note that while $\tilde{\tau}$ does not affect the value of energy at the stationary state, because $\tilde{\mathcal{F}}(\tilde{\tau}, 0) \equiv \mathcal{F}_{\rm straight}$ for all $\tilde{\tau}$, it nonetheless plays an important role in assessing the stability of the straight configuration.

When evaluated at $\alpha = 0$, for arbitrary $\tilde{\tau}$, the trace and determinant of the Hessian read,

$$\operatorname{tr}\mathcal{H}(\tilde{\tau},0) = \Lambda^2 - \Lambda^{-1} + m^2\Lambda - 2m\tilde{\tau} + \frac{1}{4}\Lambda^{-1}\tilde{\tau}^2 \quad \text{and} \quad \det\mathcal{H}(\tilde{\tau},0) = 0, \tag{3.28}$$

respectively. Because $\det\mathcal{H}(\tilde{\tau}, 0) = 0$, the straight configuration can be, at best, only *marginally stable* in the class of helicoids: a proper assessment of the stability of the straight cord would therefore require testing the second variation against a broader class of admissible perturbations, which is beyond the scope of the current analysis.

The minimum of $\operatorname{tr}\mathcal{H}(\tilde{\tau}, 0)$ is $\operatorname{tr}\mathcal{H}(\tilde{\tau}_h, 0) = 3m^2\Lambda + \Lambda^2 - \Lambda^{-1}$, obtained at $\tilde{\tau} = \tilde{\tau}_h := 4m\Lambda$. It follows that the straight, twisted neo-Hookean cord is marginally stable as long as the non-dimensional torque m is such that

$$m < m_{\rm cr} := \frac{\sqrt{\Lambda - \Lambda^{-2}}}{\sqrt{3}}. \tag{3.29}$$

Note that $m_{\rm cr}$ is less than the torque $m_P = \sqrt{\Lambda - \Lambda^{-2}}$, under which the cord is in axial compression, see equation (3.16). Hence, in agreement with experiments, the straight cord becomes unstable while the cord is still under axial tension, despite the Poynting effect's tendency to decrease the tension with the twist [34].

We now show that it is precisely when the torque reaches the computed value $m_{\rm cr}$, that is, when the straight cord becomes unstable, that the helicoid becomes energetically favourable.

(ii) Emergence of a stable helicoid

First, we check from equations (3.24) that when $m = m_{\rm cr}$, we have $\alpha_h = 0$, confirming that helicoids start smoothly out of the straight configuration. Then, as m increases beyond the critical torque $m_{\rm cr}$, both α_h and τ_h increase, see figure 4. In the limit $m \to \infty$, we have $\alpha_h \to \pi/2$, which is a purely theoretical upper bound because the chosen ansatz is inadequate at high stretches and because of close packing constraints [35]. This trend is consistent with the expectation that in

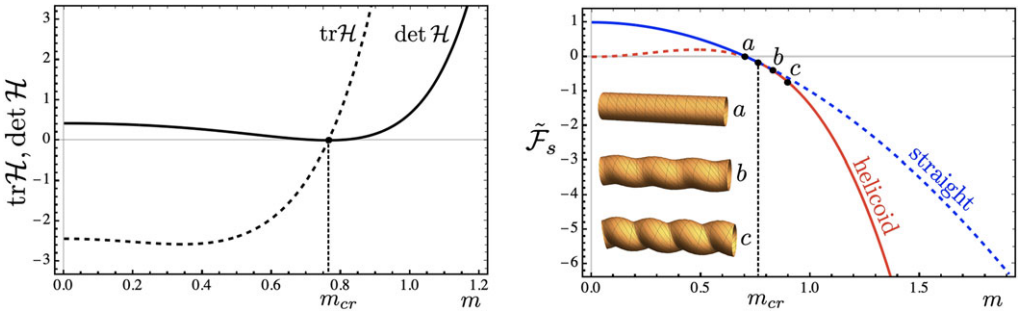

Figure 5. Left: Trace and determinant of the Hessian equation (3.27), evaluated at the stationary state equations (3.24) as a function of m. Right: Total potential energy $\tilde{\mathcal{F}}_s$ evaluated at the stationary states. Blue refers to the straight cord, red refers to the helicoid. Solid and dashed curves define stable and unstable regions, respectively, and a, b, c refer to $m = 0.75, 0.78, 0.82$, respectively. All plots are for a neo-Hookean cord with axial pre-stretch $\Lambda = 2.0$, so that $m_{\rm cr} = 0.76$.

a highly twisted rubber cord, the generatrices become increasingly tilted until they approach a perpendicular orientation to the helicoid axis, see figure 1a.

We now evaluate the invariants of the Hessian at the stationary state, $\operatorname{tr}\mathcal{H}(\tilde{\tau}_h, \alpha_h)$ and $\det\mathcal{H}(\tilde{\tau}_h, \alpha_h)$. Because the resulting expressions are lengthy and not particularly enlightening, we only display the outcomes numerically for the neo-Hookean cord, see the plots on figure 5 (left-hand panel), obtained when $\Lambda = 2.0$. We see that $\det\mathcal{H}(\tilde{\tau}_h, \alpha_h) \geq 0$ for all values of (m, Λ), attaining the zero value only at $m = m_{\rm cr}$, and that $\operatorname{tr}\mathcal{H}(\tilde{\tau}_h, \alpha_h)$ changes sign from negative to positive at $m = m_{\rm cr}$. This shows that helicoids are *unstable* for $m < m_{\rm cr}$ and *stable* for $m > m_{\rm cr}$, and that the critical torque $m_{\rm cr}$ marks the transition point from the stable straight twisted cord to the stable helicoid.

This behaviour is corroborated by comparing the total potential energy of the stationary straight and helicoidal states, $\tilde{\mathcal{F}}_s$, for fixed axial pre-stretch Λ and varying torque m. As shown in figure 5 (right-hand panel), for $m < m_{\rm cr}$, the helicoidal state has lower energy but remains unstable, while the straight state is stable. Conversely, for $m > m_{\rm cr}$, the helicoidal state becomes stable and retains lower energy than the straight state.

Note that the helicoid's pitch L and semi-amplitude ϱ are

$$L = 2\pi A \frac{\cos\alpha_h}{\tilde{\tau}_h} \quad \text{and} \quad \varrho = A\frac{\Lambda \sin\alpha_h}{\tilde{\tau}_h}, \tag{3.30}$$

in general. At the critical torque $m = m_{\rm cr}$, the initial pitch and amplitude are

$$L_0 = A\frac{\pi\sqrt{3}}{2\sqrt{\Lambda^3 - 1}} \quad \text{and} \quad \varrho_0 = 0. \tag{3.31}$$

Then the pitch decreases and the amplitude increases with m: these findings, also represented in the inset of figure 5 (right-hand panel), are consistent with experiments on rubber cords. Remarkably, the problem reveals that the ratio L_0/A, between the initial pitch at the onset of instability and the cord's reference radius, depends on the axial pre-stretch (at least in the case of a neo-Hookean material). This finding would be interesting to test experimentally, although accurately identifying the precise onset of the straight-to-helicoid instability may prove challenging in practice.

We note that although the derivation presented here can go beyond the onset of buckling, the validity of the uniform helicoidal ansatz is naturally bounded by several factors. First, as the cord undergoes extreme deformations, the assumption of a circular cross-section may weaken owing to significant warping and nonlinear constitutive effects [36]. Second, the configuration is subject to a geometric upper bound dictated by the closely packed limit of the helicoid [24,37]. Finally, experimental evidence suggests that the uniform helicoid typically loses stability to localized deformations and knot formation before these close-packing geometric limits are reached,

although there are cases where the close-packing state remains stable before the formation of a knot [38]. The current model thus characterizes the fundamental helicoidal geometry of the cord, while the complex transition toward localized knotting remains a subject for further numerical or non-uniform analytical study.

(c) Straight-to-helicoid transition: Mooney–Rivlin materials

The analysis of the straight to the helicoid bifurcation is now repeated for Mooney–Rivilin materials. The analysis is of course identical—and indeed, includes as a special case the analysis done above for neo-Hookean materials—but because of the presence of the second strain invariant I_2 in the energy functional, the resulting expressions and calculations are less transparent. At the same time, adding a dependency on the second invariant I_2 allows a better fit with experiments, and also discloses a richer arena of behaviours than the neo-Hookean model.

The strain energy density of a Mooney–Rivlin solid is in the form

$$W = C_1(I_1 - 3) + C_2(I_2 - 3), \tag{3.32}$$

where C_1, C_2 are positive constants. We introduce the ratio $c = C_2/C_1$, which may take any value between 0 (neo-Hookean model) and ∞ (extreme Mooney model). For this model, the initial shear modulus is $\mu = 2(C_1 + C_2) = 2C_1(1 + c)$.

Upon calculating the second invariant of $\mathbf{C}$ and integrating over the cylinder's volume, as we did in equation (2.20) in the neo-Hookean ($c = 0$) case, we obtain the elastic energy density per length unit as (up to an inessential constant) as

$$\begin{aligned} e = \frac{E}{\mu H A^2 \pi} &= \frac{1}{2(1+c)}[\lambda^2 + 2\lambda^{-1} - 3 + c(\lambda^{-2} + 2\lambda - 3)] \\ &+ \frac{1}{8}\lambda^{-2}(\lambda + 2c)\tilde{\kappa}^2 + \frac{1}{4}\lambda^{-2}(\lambda + c)(\tilde{\gamma} + \tilde{\tau})^2. \end{aligned} \tag{3.33}$$

Initially we look at the behaviour of a straight cord with axial pre-stretch Λ, subjected to the torque m and under axial tension f. In this case, we set $\tilde{\kappa} = \tilde{\tau} = 0$ in the expression of the energy density, and we consider the total potential energy equation (3.12),

$$\mathcal{F}(\lambda, \tilde{\gamma}, f) = e - f(\lambda - \Lambda) - m\tilde{\gamma}, \tag{3.34}$$

where the non-dimensional axial load f and torque $m \equiv m_t$ are given again by equations (3.4). From the stationarity conditions,

$$\frac{\partial \mathcal{F}}{\partial \lambda} = 0, \quad \frac{\partial \mathcal{F}}{\partial f} = 0 \quad \text{and} \quad \frac{\partial \mathcal{F}}{\partial \tilde{\gamma}} = 0, \tag{3.35}$$

we obtain the equilibrium values of $\lambda, f, \tilde{\gamma}$. In particular, we find that the axial traction is tensile as long as the torque is less than

$$m_P = \frac{(c + \Lambda)^{3/2}}{(1 + c)\Lambda^2}\sqrt{\frac{\Lambda^3 - 1}{2c + \Lambda}}, \tag{3.36}$$

in agreement with Rivlin's formula for a stretched Mooney–Rivlin cylinder under torsion [33,34].

To compute the value of the torque above which a straight twisted cord of Mooney–Rivlin solid becomes unstable and transitions to the helicoidal shape, we extend the calculations of §3b(ii) to the energy equation (3.33). Hence we study the stationary points of the total potential energy $\bar{\mathcal{F}}(\tilde{\gamma}, \tilde{\tau}, \alpha) = e(\tilde{\gamma}, \tilde{\tau}, \alpha) - m_t\tilde{u}_3 - m_b\tilde{\kappa}$ with e given by equation (3.33), wherein we have set again $\lambda = \Lambda\sqrt{\tilde{\kappa}^2 + \tilde{\tau}^2}/\tilde{\tau}$. From the conditions

$$\frac{\partial \bar{\mathcal{F}}}{\partial \tilde{\gamma}} = 0 \quad \text{and} \quad \frac{\partial \bar{\mathcal{F}}}{\partial \tilde{\tau}} = 0, \tag{3.37}$$

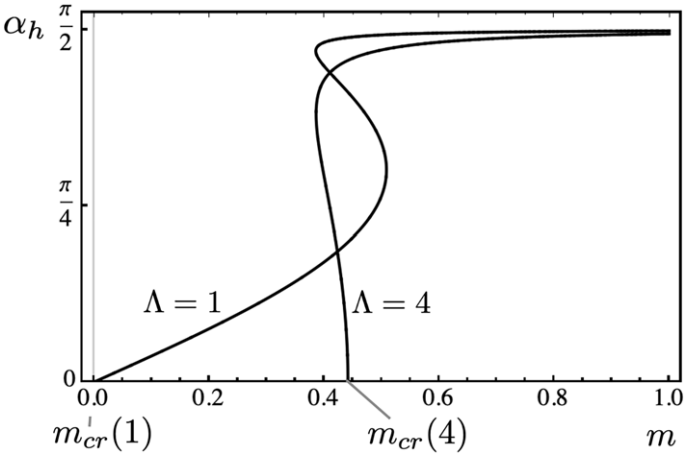

Figure 6. Slope of the helicoid's centreline α_h as a function of the applied torque m and of the axial pre-stretch Λ for Mooney–Rivlin materials. Here $c = 10$.

we find

$$\tilde{\gamma}_h = -\frac{2(1+c)m\Lambda^3}{(\Lambda + c\cos\alpha_h)(\Lambda + 2c\cos\alpha_h)} \quad \text{and} \quad \tilde{\tau}_h = \frac{4(1+c)m\Lambda^2}{\Lambda + 2c\cos\alpha_h}. \tag{3.38}$$

The value of α_h follows from the last stationarity condition,

$$\frac{\partial \bar{\mathcal{F}}}{\partial \tilde{\alpha}} = 0. \tag{3.39}$$

Upon inserting equations (3.38) into equation (3.39), this condition can be rewritten in the form

$$m = \hat{m}(\alpha_h, \Lambda). \tag{3.40}$$

The explicit expression of $\hat{m}$ is unwieldy and is not reproduce here, but it remains fully analytical. With m and Λ treated as control parameters, equations (3.40) and (3.38) yield the triplet $(\tilde{\gamma}_h, \tilde{\tau}_h, \alpha_h)$ that characterizes the helicoidal configurations rendering the total potential stationary. Note that these expressions involve no smallness assumptions on the control parameters, and provide the exact analytical description of the post-buckled helicoid.

The plot of α_h versus m for various values of Λ reveals a richer structure than in the neo-Hookean case. In particular, some parameter ranges now exhibit a genuine snap-through behaviour between distinct buckled states. Figure 6 shows that, for $\Lambda = 1$ and m in the interval $(0.4, 0.5)$, three helicoidal configurations coexist. It can be shown that the configuration with the largest winding (i.e. the highest α_h) minimizes the total potential energy. Yet this state may be physically unattainable owing to close-packing constraints. Although these features are intriguing and potentially relevant in applications, a detailed analysis is deferred to future studies.

We now we look for the emergence of helicoidal configurations, in their incipient branching out of the straight state. We set $\alpha_h = 0$ in equation (3.40), which leads to the expression of the critical torque,

$$m_{\mathrm{cr}}(\Lambda) := \hat{m}(0, \Lambda) = \frac{(c+\Lambda)^{3/2}}{(1+c)\Lambda^2}\sqrt{\frac{(2c+\Lambda)(\Lambda^3-1)}{4c^2+6c\Lambda+3\Lambda^2}}. \tag{3.41}$$

To show that this is precisely the value of the torque below which the straight cord remains marginally stable, we compute the 3×3 Hessian,

$$\mathcal{H}_3(\tilde{\gamma}, \tilde{\tau}, \alpha) = \begin{bmatrix} \tilde{\mathcal{F}}_{,\tilde{\gamma}\tilde{\gamma}} & \tilde{\mathcal{F}}_{,\tilde{\gamma}\tilde{\tau}} & \tilde{\mathcal{F}}_{,\tilde{\gamma}\alpha} \\ \tilde{\mathcal{F}}_{,\tilde{\tau}\tilde{\gamma}} & \tilde{\mathcal{F}}_{,\tilde{\tau}\tilde{\tau}} & \tilde{\mathcal{F}}_{,\tilde{\tau}\alpha} \\ \tilde{\mathcal{F}}_{,\alpha\tilde{\gamma}} & \tilde{\mathcal{F}}_{,\alpha\tilde{\tau}} & \tilde{\mathcal{F}}_{,\alpha\alpha} \end{bmatrix}, \tag{3.42}$$

and we study its positivity through the sign of its invariants

$$\mathcal{I}_1 = \operatorname{tr}\mathcal{H}_3, \quad \mathcal{I}_2 = \frac{1}{2}[(\operatorname{tr}\mathcal{H}_3)^2 - \operatorname{tr}(\mathcal{H}_3^2)] \quad \text{and} \quad \mathcal{I}_3 = \det\mathcal{H}_3. \tag{3.43}$$

We now evaluate the Hessian at the straight state which, as previously noted, is itself a stationary point of the energy within the class of helicoids. Setting $\alpha_h = 0$ in equations (3.38), we find that the Hessian and its invariants depend only on the parameters (m, Λ). In particular, for all values of control parameters we find that

$$\mathcal{I}_3 = 0, \tag{3.44}$$

showing that, as in the neo-Hookean case, the straight configuration is at best marginally stable when probed with helicoidal perturbations. Again, we note that full assessment of strict stability would require testing a broader class of perturbations, which is standard in bifurcation analyses, but this lies beyond the scope of the present work.

Imposing the remaining positivity conditions for the Hessian when evaluated at the straight state,

$$\mathcal{I}_1 > 0 \quad \text{and} \quad \mathcal{I}_2 > 0, \tag{3.45}$$

we deduce that the admissible values of (m, Λ) must satisfy

$$m < m_{\mathrm{cr}} := \frac{(c+\Lambda)^{3/2}}{(1+c)\Lambda^2}\sqrt{\frac{(2c+\Lambda)(\Lambda^3-1)}{4c^2+6c\Lambda+3\Lambda^2}}. \tag{3.46}$$

Here, m_{cr} is precisely the torque that renders the energy stationary in the straight cord, thus justifying the attribute *critical*. This result extends the neo-Hookean analysis, confirming that the straight state loses stability (under helicoidal perturbations) once the applied torque exceeds m_{cr}. As expected, setting $c = 0$ recovers the neo-Hookean critical threshold.

Note that while the occurrence of the snap-through instability in the twisted cord, as the ones described here for Mooney–Rivlin materials, still awaits experimental characterization, the phenomenon is consistent with similar instabilities observed in this material class for inflated rubber balloons and electroactive polymers [16].

4. Comparison with experiments

The theory developed in this work can be assessed by comparison with experiments on instabilities in slender rubber cords subjected to axial pre-stretch and torsion. This comparison, however, presents practical difficulties because, as shown in the previous section, the amplitude of the helicoid at the onset of instability is initially equal to zero and then increases smoothly with the torque, so that it is quite difficult to capture experimentally the precise instant when a straight cord starts to develop helicoidal configurations.

It is much easier, as suggested in the seminal work by Gent & Hua [23], to measure the moment at which a knot forms. In soft cords like the ones we consider here, this instability generally occurs much later in the onset of the helicoid, therefore we expect that our analysis should provide a lower critical load than the one required to form a knot.

To compare our results with available experimental data we use the *critical torsion factor* (ϕA) used in experiments on rubber cords in [23,38], where by making reference to the straight cord, $\phi = \Delta\varphi/h$ with $\Delta\varphi$ the relative rotation between the upper and lower faces of the cylinder and h its current length. We have

$$\gamma = \frac{\Delta\varphi}{H} = \frac{\Delta\varphi}{h}\frac{h}{H} = \Lambda\phi, \tag{4.1}$$

and because $\tilde{\gamma} = \gamma A$, it follows that $(\phi A) = \tilde{\gamma}\Lambda^{-1}$. We recall from equation $(3.14)_3$, that as long as the cord is straight, we have $\tilde{\gamma} = 2m\Lambda$, so that the torsion factor can be obtained from the dimensionless torque as $(\phi A) = 2m$.

To establish a meaningful comparison with experiments, we use the Mooney–Rivlin model as it covers the full class of materials described by third-order elasticity. Using the values of the

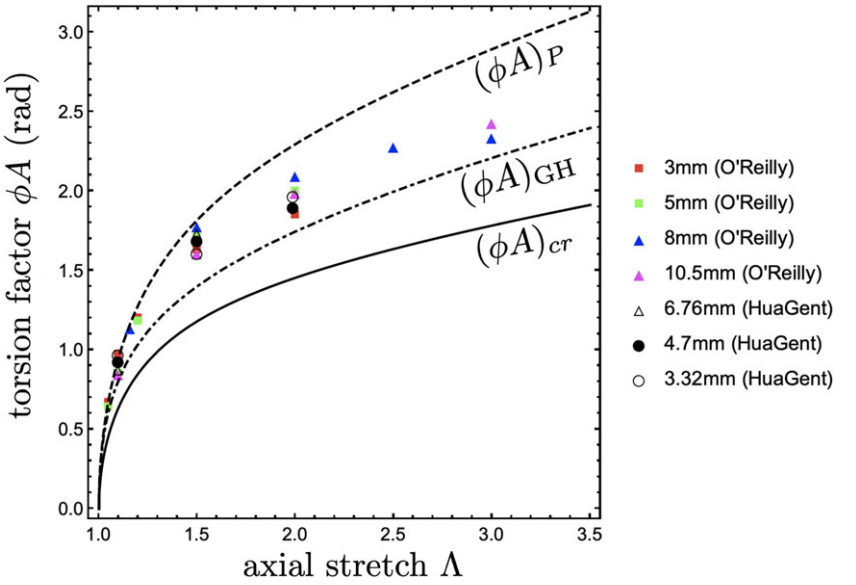

Figure 7. Comparison of the predicted theoretical values of the critical torsion factor for the onset of helicoidal configurations $(\phi A)_{\rm cr}$ and for the onset of axial compression $(\phi A)_P$ for Mooney–Rivlin solids with $c = C_2/C_1 = 0.22$, versus experimental values of the torsion factor (ϕA) relative to the formation of the first knot in axially pre-stretched cords with different diameters. Also represented is the theoretical estimate $(\phi A)_{\rm GH}$ of Gent & Hua [23] for the formation of the first knot in a neo-Hookean cord ($c = 0$).

critical torque m_P for the onset of axial compression equation (3.36), and of the critical torque $m_{\rm cr}$ for the onset of the helicoidal state equation (3.41), we find the corresponding torsion factors as

$$(\phi A)_P = 2\frac{(c+\Lambda)^{3/2}}{(1+c)\Lambda^2}\sqrt{\frac{\Lambda^3-1}{2c+\Lambda}} \quad \text{and} \quad (\phi A)_{\rm cr} = 2\frac{(c+\Lambda)^{3/2}}{(1+c)\Lambda^2}\sqrt{\frac{(2c+\Lambda)(\Lambda^3-1)}{4c^2+6c\Lambda+3\Lambda^2}}. \tag{4.2}$$

The value of the dimensionless parameter c is the only constitutive parameter required to link (ϕA) and Λ. This piece of information can be extracted from uniaxial tension experiments described in [38], on polyurethane cords with diameters ranging from 3 to 10.5 mm. We find c in the range $(0.22, 0.30)$, and here we set $c = 0.22$.

Comparisons between theory and the experimental findings of [23,38] are reported in figure 7. They show that the straight-to-helicoid transition consistently anticipates the onset of knots, over a large range of axial pre-stretch Λ. The plot also shows that helicoids and knots mostly form when the cable is still axially tensioned, with a few outliers for thinner cords at lower values of pre-stretch.

A comment is in order relative to the slenderness of the cord. Our experimental observations indicate that boundary clamping effects are localized within regions approximately 5–10 times the stretched diameter of the cord. Beyond these extinction zones, the helical amplitude and wavelength remain uniform, provided no localizations such as knotting occur. While geometric and constitutive nonlinearities make analytical estimates of these zones difficult without numerical methods [24], the bulk of the cord remains well-characterized by the uniform model described in this work.

5. Conclusion

We have shown that the emergence of helicoidal states in twisted and axially pre-stretched cords modelled by the neo-Hookean and Mooney–Rivlin strain energies can be studied algebraically, as

long as we focus on the emergence of uniform, non-straight configurations and provided the end effects owing to clamping can be neglected. This approach provides analytical expressions for the critical values of the torque that are required for a straight cord to become unstable, at which point uniform helicoids appear and become energetically favourable. As the torque increases past this critical value, the helicoid's amplitude increases and its pitch decreases, in full agreement with experimental observations. As expected from available experiments, this critical torque precedes the formation of a knot.

In principle, one could expect that uniform states like the ones obtained here should be obtained as special cases of the more general solution to the ordinary differential equations describing the equilibrium of hyperelastic cords made of incompressible, hyperelastic material (see [24,36]). Importantly, our simplified energy-based framework highlights how three-dimensional material responses, such as the Poynting effect, can influence instability thresholds in a way that cannot be resolved within Cosserat or Kirchhoff rod models. While our analysis neglects boundary layers and non-uniform patterns, it nevertheless provides a tractable ansatz for capturing the first stage of instability, bridging the gap between exact differential formulations and experimentally observed transitions. In this sense, our approach could be useful in devising a simplified treatment of problems wherein the configuration of twisted cords are made of finite regions of uniform states, as those described in [24,37,39], for example.

Future work could extend this algebraic framework to account for localized instabilities, non-circular cross-sections and finite-length effects, for which nonlinear ordinary-differential-equation-based methods and numerical simulations remain indispensable. Beyond rubber cords, our results may also prepare the study of twisted soft filaments in biological and technological settings, from actin bundles to self-assembled nanostructures, where helicoidal transitions play a crucial mechanical role.

Data accessibility. This article does not contain any additional data.

Declaration of AI use. We have not used AI-assisted technologies in creating this article.

Authors' contributions. G.Z.: conceptualization, formal analysis, methodology, writing—original draft; M.D.: conceptualization, formal analysis, methodology, writing—original draft.

Both authors gave final approval for publication and agreed to be held accountable for the work performed therein.

Conflict of interest declaration. We declare we have no competing interests.

Funding. The origin of this work can be traced back to an undergraduate Final Year Project that took place at University College Dublin in 2010. It was conducted by Fintan O'Reilly [38] and supervised by Michel Destrade (M.D.) and Michael Gilchrist at the School of Materials and Mechanical Engineering. The latter was the host scientist for M.D.'s 2008–2010 Senior Marie Curie Fellowship, awarded by the Seventh Framework Programme of the European Commission to the BIOMECH project (grant agreement no. ID: 219800).

Acknowledgements. We gratefully acknowledge the technical help of undergraduate student Tomás Gillanders at the University of Galway, who devised and implemented an optical device to capture the onset of helicoidal instabilities, as illustrated in figure 1, during a summer internship at the School of Mathematical and Statistical Sciences in 2023.

References

1. Chouaieb N, Goriely A, Maddocks JH. 2006 Helices. *Proc. Natl Acad. Sci. USA* **103**, 9398–9403. (doi:10.1073/pnas.0508370103)
2. Galloway JW. 2001 Helical imperative: paradigm of form and function. In *Encyclopedia of life sciences*. New York: Wiley.
3. Coleman BD, Swigon D. 2004 Theory of self-contact in Kirchhoff rods with applications to supercoiling of knotted and unknotted DNA plasmids. *Phil. Trans. R. Soc. Lond. A* **362**, 1281–1299. (doi:10.1098/rsta.2004.1393)
4. Maritan A, Micheletti C, Trovato A, Banavar JR. 2000 Optimal shapes of compact strings. *Nature* **406**, 287–290. (doi:10.1038/35018538)
5. Bouzar L, Müller MM, Messina R, Nöding B, Köster S. 2019 Helical superstructure of intermediate filaments. *Phys. Rev. Lett.* **122**, 098101. (doi:10.1103/PhysRevLett.122.098101)

6. Leijnse N, Oddershede LB, Bendix PM. 2015 Helical buckling of actin inside filopodia generates traction. *Proc. Natl Acad. Sci. USA* **112**, 136–141. (doi:10.1073/pnas.1411761112)
7. Goriely A, Tabor M. 1998 Spontaneous helix hand reversal and tendril perversion in climbing plants. *Phys. Rev. Lett.* **80**, 1564–1567. (doi:10.1103/PhysRevLett.80.1564)
8. Silverberg JL, Noar RD, Packer MS, Harrison MJ, Henley CL, Cohen I, Gerbode SJ. 2012 3D imaging and mechanical modeling of helical buckling in *Medicago truncatula* plant roots. *Proc. Natl Acad. Sci. USA* **109**, 16 794–16 799. (doi:10.1073/pnas.1209287109)
9. Srivastava S *et al.* 2010 Light-controlled self-assembly of semiconductor nanoparticles into twisted ribbons. *Science* **327**, 1355–1359. (doi:10.1126/science.1177218)
10. Kirchhoff G. 1859 Über das Gleichgewicht und die Bewegung eines unendlich dünnen elastischen Stabes. *J. Reine Angew. Math.* **56**, 285–313.
11. Chouaieb N, Maddocks JH. 2004 Kirchhoff's problem of helical equilibria of uniform rods. *J. Elast.* **77**, 221–247. (doi:10.1007/s10659-005-0931-z)
12. Goriely A. 2018 *The mathematics and mechanics of biological growth*. New York: Springer.
13. Moulton DE, Lessinnes T, Goriely A. 2013 Morphoelastic rods I: a single growing elastic rod. *J. Mech. Phys. Solids* **61**, 398–427. (doi:10.1016/j.jmps.2012.09.017)
14. Moulton DE, Lessinnes T, Goriely A. 2020 Morphoelastic rods III: differential growth and curvature generation in elastic filaments. *J. Mech. Phys. Solids* **142**, 104022. (doi:10.1016/j.jmps.2020.104022)
15. Neukirch S, van der Heijden GHM, Thompson JMT. 2002 Writhing instabilities of twisted rods: from infinite to finite length. *J. Mech. Phys. Solids* **50**, 1175–1191. (doi:10.1016/S0022-5096(01)00130-2)
16. Destrade M, Zurlo G. 2025 *Nonlinear elasticity: a concise masterclass for undergraduates*. New York: Springer.
17. Antman SS. 1995 *Nonlinear problems of elasticity*. New York: Springer.
18. Audoly B, Lestringant C. 2021 Asymptotic derivation of high-order rod models from non-linear 3D elasticity. *J. Mech. Phys. Solids* **148**, 104264. (doi:10.1016/j.jmps.2020.104264)
19. Mora MG, Müller S. 2003 Derivation of the nonlinear bending-torsion theory for inextensible rods by Γ-convergence. *Calc. Var.* **18**, 287–305. (doi:10.1007/s00526-003-0204-2)
20. Neukamm S. 2012 Rigorous derivation of a homogenized bending-torsion theory for inextensible rods from three-dimensional elasticity. *Arch. Rat. Mech. Anal.* **206**, 645–706. (doi:10.1007/s00205-012-0539-y)
21. Scardia L. 2009 Asymptotic models for curved rods derived from nonlinear elasticity by Γ-convergence. *Proc. R. Soc. Edinb. A* **139**, 1037–1070. (doi:10.1017/S0308210507000194)
22. Ericksen JL. 1970 Simpler static problems in nonlinear theories of rods. *Int. J. Solids Struct.* **6**, 371–377. (doi:10.1016/0020-7683(70)90045-4)
23. Gent AN, Hua K-C. 2004 Torsional instability of stretched rubber cylinders. *Int. J. Non-Linear Mech.* **39**, 483–489. (doi:10.1016/S0020-7462(02)00217-2)
24. Liu L, Liu H, He Y, Liu D. 2024 Mechanics and topology of twisted hyperelastic filaments under prescribed elongations: experiment, theory, and simulation. *J. Mech. Phys. Solids* **182**, 105478. (doi:10.1016/j.jmps.2023.105478)
25. Domokos G, Healey TJ. 2005 Multiple helical perversions of finite, intrinsically curved rods. *Int. J. Bifurcat. Chaos* **15**, 871–890. (doi:10.1142/S0218127405012430)
26. Healey TJ, Papadopoulos CM. 2013 Bifurcation of hemitropic elastic rods under axial thrust. *Q. Appl. Math.* **71**, 729–753. (doi:10.1090/S0033-569X-2013-01308-7)
27. Zurlo G, Blackwell J, Colgan N, Destrade M. 2020 The Poynting effect. *Am. J. Phys.* **88**, 1036. (doi:10.1119/10.0001997)
28. Fosdick RL, MacSithigh G. 1986 Minimization in incompressible nonlinear elasticity theory. *J. Elast.* **16**, 267–302. (doi:10.1007/BF00040817)
29. Fosdick RL, Zhang Y. 1993 The torsion problem for a nonconvex stored energy function. *Arch. Rat. Mech. Anal.* **122**, 291–322. (doi:10.1007/BF00375138)
30. Deseri L, Piccioni MD, Zurlo G. 2008 Derivation of a new free energy for biological membranes. *Continuum Mech. Thermodyn.* **20**, 255–273. (doi:10.1007/s00161-008-0081-1)
31. Favata A, Paroni R, Recrosi F, Tomassetti G. 2022 Competition between epithelial tissue elasticity and surface tension in cancer morphogenesis. *Int. J. Eng. Sci.* **176**, 103677 (doi:10.1016/j.ijengsci.2022.103677)
32. Destrade M, Gilchrist MD, Murphy JG. 2010 Onset of nonlinearity in the elastic bending of blocks. *ASME J. Appl. Mech.* **77**, 061015. (doi:10.1115/1.4001282)

33. Rivlin RS. 1949 Large elastic deformations of isotropic materials VI. Further results in the theory of torsion, shear and flexure. *Phil. Trans. R. Soc. Lond. A* **242**, 173–195. (doi:10.1098/rsta.1949.0009)
34. Kanner LM, Horgan CO. 2008 On extension and torsion of strain-stiffening rubber-like elastic circular cylinders. *J. Elast.* **93**, 39–61. (doi:10.1007/s10659-008-9164-2)
35. Olsen K, Bohr J. 2010 The generic geometry of helices and their close-packed structures. *Theor. Chem. Acc.* **125**, 207–215. (doi:10.1007/s00214-009-0639-4)
36. DiCarlo A, Nardinocchi P. 1998 On the torsion of soft cylindrical shells. In *Proc. of the Symp. on Trends in Applications of Mathematics to Mechanics (STAMM98)*. Milan Berlin Heidelberg New York: Springer.
37. Charles N, Gazzola M, Mahadevan L. 2019 Topology, geometry, and mechanics of strongly stretched and twisted filaments: solenoids, plectonemes, and artificial muscle fibers. *Phys. Rev. Lett.* **123**, 208003. (doi:10.1103/PhysRevLett.123.208003)
38. O'Reilly F. 2010 Twisting instabilities of highly deformable cylinders. Final year project dissertation, University College Dublin, Ireland. Project Supervisors: M.D. Gilchrist, M. Destrade.
39. Dilly É, Neukirch S, Derr J, Zanchi D. 2023 Traveling perversion as constant torque actuator. *Phys. Rev. Lett.* **131**, 177201. (doi:10.1103/PhysRevLett.131.177201)